International Journal of Mass Spectrometry 435 (2019) 259–271

Contents lists available at ScienceDirect

International Journal of Mass Spectrometry

journal homepage: www.elsevier.com/locate/ijms

Full Length Article

Probing arginine-phosphopeptide interactions in non-covalent peptide-peptide ion complexes using gas-phase cross-linking and Born-Oppenheimer molecular dynamics calculations

Huong T.H. Nguyen, Shu Rong Huang, Yang Liu, Yue Liu, Joseph A. Korn, František Tureček*

Department of Chemistry, Box 351700, University of Washington, Seattle, WA, 98195-1700, United States

ARTICLE INFO

Article history:
Received 15 June 2018
Received in revised form
19 September 2018
Accepted 28 September 2018
Available online 3 November 2018

Dedicated to Professor Helmut Schwarz on the occasion of his 75th birthday.

Keywords:
Arginine-phosphopeptide complexes
Photodissociative crosslinking
Sequence analysis
Ion structures
Born-Oppenheimer molecular dynamics

ABSTRACT

We report a study of non-covalent complexes of phosphopeptides pXAAAA and *N*-Ac-pXAAAA (X = Ser, Thr, Tyr) with arginine-containing peptides carrying diazirine 4,4-azipentyl tags at the *N*-terminus, *LGG(A)$_n$R, or in the photoleucine residue, L*GG(A)$_n$R (n = 3–5). Complexes with *LGG(A)$_n$R were successfully generated as singly charged ions in the gas phase in 0.6–3.5% yields. In contrast, complexes with L*GG(A)$_n$R were formed in negligible (<0.1%) yields. Selective photodissociation at 355 nm of the diazirine ring in [*LGG(A)$_n$R + pXAAAA + H]$^+$ ions resulted in loss of N_2, producing large (75–95%) fractions of non-dissociating complexes that were further probed by collision-induced dissociation tandem mass spectrometry (CID-MS^3). Covalent cross-links in the complexes produced by photoinduced carbene insertion were identified by specific CID-MS^3 dissociations involving H_3PO_4 transfer and backbone fragmentations. *N*-acetylation in the phosphopeptides was found to have a substantial negative effect on the formation of covalent cross-links. Amongst the phosphorylated amino acid residues, pTyr showed the highest tendency (up to 92%) to form covalent cross-links. The fractions of covalent cross-links substantially increased with the length of the photopeptide chain. Born-Oppenheimer molecular dynamics (BOMD) calculations of canonical and zwitterionic protomers of the (pYAAAA + *LGGAAAR + H)$^+$ complex indicated multiple close contacts between the incipient carbene of the diazirine ring and the X—H bonds (X═C, N, O) in the phosphopeptide. BOMD in combination with structural analysis by density functional theory calculations were used to interpret the experimental data and explain the cross-linking efficiencies.

1. Introduction

Reversible protein phosphorylation [1] is one of the most important post-translational modifications that plays a critical role in regulating many cellular processes including cell cycle, cell growth, and cell signal transduction pathways. Although the mechanism of reversible protein phosphorylation has been studied intensively [2], the importance for protein structure and functioning of non-covalent binding of phosphopeptides to lysine and arginine residues in proteins [3] and simpler models continues to stimulate investigations [4]. For example, the phosphotyrosine binding region SH2 of Src proteins, that has been characterized by high-resolution methods such as X-ray crystallography [5] and NMR spectroscopy [6], has also been the subject of mass spectrometry studies [7]. Loo and coworkers have shown that non-covalent phosphopeptide complexes with the Src homology 2 domain protein could be produced by electrospray ionization and studied by mass spectrometry [8]. Likewise, binding of arginine-rich peptides to RNA has been studied by electrospray ionization mass spectrometry and the complex ion formation in the gas phase was correlated with the known binding properties in solution [9]. Non-covalent complexes of arginine-rich peptides with phosphorylated peptides have been produced by soft ionization methods and shown to be stable in the gas phase [10,11]. In addition, collision-induced dissociation (CID) of arginine-phosphate non-covalent complexes produced fragment ions by covalent-bond cleavages while the non-covalent interactions were in part preserved intact [12,13]. These results pointed to the importance of strong non-covalent interactions of the arginine-phosphate type in the gas phase. However, interpretation of the mass spectrometric data did not provide spe-

* Corresponding author.
E-mail address: turecek@chem.washington.edu (F. Tureček).

https://doi.org/10.1016/j.ijms.2018.09.037
1387-3806/

cific information about the equilibrium structure of non-covalent complexes or their dynamics.

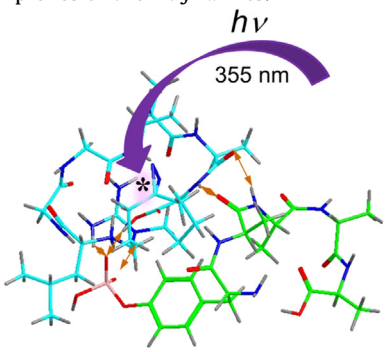

Recently, we have combined experimental studies of photodissociative cross-linking in the gas phase with Born-Oppenheimer molecular dynamics (BOMD) calculations as a new approach to probing non-covalent binding in peptide-peptide ion complexes produced by electrospray ionization. The chemical nature of our photodissociative cross-linking method relies on diazirine tags that are incorporated in synthetic peptides. The amino acid residues that can be selectively tagged in the side chain include leucine (L-2-amino-4,4-azi-pentanoic acid, called photoleucine, L*) [14], a methionine analog (L-2-amino-5,5-azi-hexanoic acid, photomethionine, M*) [14], and lysine (L-2,6-diamino-4,4-azi-hexanoic acid) [15]. In addition to these, the lysine ε-amino group (K*), leucine *N*-terminus (*L) [16], and the cysteine thiol group (C*) in peptides [17] have been selectively tagged with the 4,4-azi-1-pentyl group and used in gas-phase cross-linking [16–19]. The diazirine ring undergoes selective photodissociative loss of N_2 by irradiation at 330–370 nm [20], which is a region where natural peptide or protein chromophores are transparent [21]. Diazirine photodissociation creates a transient singlet carbene which either reacts by insertion into a proximate X—H bond in the complex or competitively self-destructs by intramolecular isomerization by 1,2-hydrogen shift from the adjacent methyl or methylene groups, forming nonreactive olefins.

These competitive side reactions have very low activation energies as established for peptide ions [22] (19–31 kJ mol^{-1}, Fig. 1, left panel), resulting in fast isomerization kinetics (Fig. 1, right panel a). For typical vibrational energies in gas-phase peptide ions, as illustrated by the energy distribution curve for a model peptide (GL*GGK + 2 H)$^{2+}$ (Fig. 1, right panel b) [22], the carbene lifetimes are shorter than 10^{-7} s, providing an internal clock for the timescale of the covalent bond formation. This time scale is commensurable with that for the thermal conformational motion in the gas-phase complex that can be simulated by advanced molecular dynamics. In the absence of covalent crosslinking, the vibrational excitation provided by the highly exothermic carbene-to-olefin isomerization (ΔE_{rxn} > 200 kJ mol^{-1}, [22]) can drive complex dissociation [18,19]. In case a new covalent bond is formed, its location can potentially be located by sequencing the products in the gas phase using collision-induced dissociation spectra (CID-MS^3) [16–19].

We now apply gas-phase cross-linking to investigate non-covalent peptide-peptide complexes, consisting of phosphorylated pentapeptides, pXAAAA where X = Ser, Thr, or Tyr and their *N*-acetylated analogues, and diazirine tagged *LGG(A)$_n$R and L*GG(A)$_n$R n = 3–5 photopeptides. Our goal was to investigate the binding and structures of these complexes with regard to potential interactions of the phosphate with a single arginine residue. To investigate the conformational space and achieve atomic-level resolution in structural assignment, we used density functional theory calculations and Born-Oppenheimer molecular dynamics (BOMD) trajectory simulations with all-valence electron semiempirical quantum chemistry methods to capture the thermal motion in the (pYAAAA + *LGGAAAR + H)$^+$ complex.

2. Experimental

Peptides photo-labeled at the *N*-terminus, *LGGAAAR, *LGGAAAAR, *LGGAAAAAR, were synthesized on a CEM Liberty synthesizer. The tag was introduced by alkylating the selectively deprotected leucine *N*-terminus in a solid-phase bound peptide with 1-iodo-4,4-diazirine pentane, as described in detail previously [16]. Phosphorylated pentapeptides pTAAAA, pSAAAA, pYAAAA, and their complementary *N*-acetylated peptides (>90% purity) were purchased from Genscript (Piscataway, NJ, USA) and used as received. The other peptide library, consisting of L*GGAAAR, L*GGAAAAR, and L*GGAAAAAR, where L* was the photoleucine (L-2-amino-4,4-azi-pentanoic acid) residue, was also synthesized using a standard Fmoc solid phase procedure [23], as described previously [19]. Solutions of the complexes were prepared by mixing 50 μL of the phosphopeptide (5 – 10 μM in 50:50:1 methanol/water/acetic acid) and 100 μL of the photopeptide (5 – 10 μM in 50:50:1 methanol/water/acetic acid). The mixed solution was electrosprayed from a pulled fused silica capillary at a 1.5–2 μL/min flow rate into a linear ion trap tandem mass spectrometer, LTQ-XL ETD (ThermoElectron Fisher, San Jose, CA, USA). Photodissociation experiments at 355 nm were carried out as described previously [24,25]. Briefly, the laser beam was generated from an EKSPLA NL 301 H T (Altos Photonics, Bozeman, MT, USA) Nd-YAG laser operating at 20 Hz frequency with a 3–6 ns pulse width. The laser was interfaced with the LTQ-XL ETD mass spectrometer as described previously [26]. The typical light intensity used in the photodissociation experiments was 18 mJ/pulse. Multiple (19–39) laser pulses were used to achieve photodissociation of mass-selected ion-molecule complexes. Collision-induced dissociation (CID) spectra were obtained at 25–26 units of normalized collision energies (NCE) and with activation times that were varied between the instrument default setting of 30 ms for preliminary analysis and 1000 ms. The long activation times were chosen to match the ion storage time used in photodissociation.

3. Calculations

Born-Oppenheimer molecular dynamics (BOMD) trajectories were run with semiempirical all-valence-electron quantum chemistry calculations using the Berendson thermostat algorithm [27]. Temperature was set at 310 K to represent the experimental conditions in the ion trap. The ion system under study, (pYAAAA + *LGGAAAR + H)$^+$, was represented by three different types of protomers (Fig. 2).

In Type ***I*** complexes, the peptides had canonical ion or neutral structures with the charge located on the protonated guanidine group of the Arg residue whereas the phosphate group was neutral. Type ***II*** complexes were constructed as zwitterions with two positive charges located on the protonated guanidine group of the Arg residue and the *N*-terminus of the phosphorylated peptide while the phosphate group carried a negative charge. Type ***III*** complex were also zwitterions with two positive charges located on the protonated guanidine group of the Arg residue and the *N*-terminus of the photolabeled peptide while the phosphate group carried a negative charge (Fig. 2). For each complex type, ten initial structures were constructed from PM6-optimized peptide subunits in which the diazirine tag and pTyr were in different spatial orientations, and the complexes were optimized with semi-empirical PM6-D3H4 calculations [28]. These complexes were subjected to a preliminary BOMD using PM6-D3H4 under MOPAC [29] that was coupled

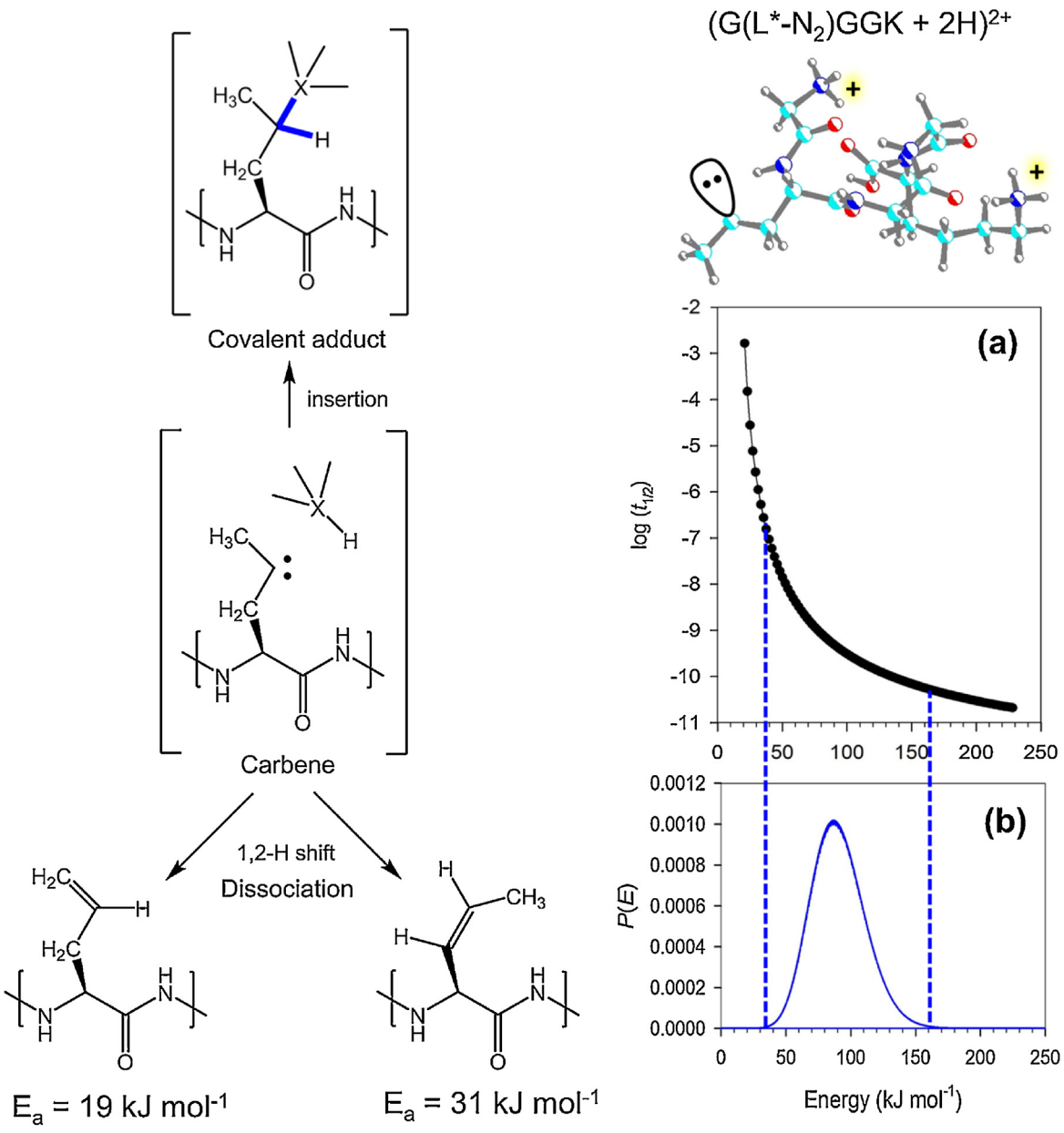

Fig. 1. Left panel: Scheme of carbene complex isomerization in (L^*-N_2) by 1,2-hydrogen migrations from adjacent methyl and methylene groups. Activation energies are from M06-2X/6-311++G(2d,p) + ZPVE calculations for the model $[G(L^*–N_2)GGK + 2\,H)^{2+}$ singlet carbene ion [22]. Right panel: (a) Calculated half-lives of the carbene for a 1,2-hydrogen migration from the methyl group. (b) Vibrational energy distribution in the singlet carbene $[G(L^*–N_2)GGK + 2\,H]^{2+}$ at 310 K.

to the Cuby4 framework [30,31]. Running trajectories with 1 fs steps for 20 ps furnished 20,000 snapshots from which 200 snapshots per structure were extracted at 100 fs intervals. The total of $200 \times 10 = 2000$ extracted snapshot structures were fully gradient-optimized with PM6-D3H4 and sorted out by energy ranking. Ten lowest-energy PM6-D3H4 structures within 40 kJ mol^{-1} were then subjected to a full BOMD with PM6-D3H4 for 100 ps. Cuby4 was also used to extract close contacts between the carbon atom of the diazirine ring and the hydrogen-carrying atoms of the phosphopeptide. Close contacts were limited to X-H. . .C distance of less than 4.5 Å on the basis of the van der Waals radii of the diazirine and X—H atoms [19]. This entire procedure was run for each Type I, II, and III protomeric complexes.

Thermochemical calculations were performed using the Gaussian 16 (Revision A.03) [32] suite of programs. Ten lowest-energy structures of each Type I-III complexes from the PM6-D3H4 calculations were re-optimized with B3LYP/6–31 G(d,p) [33] to provide harmonic frequencies that were used to evaluate enthalpies, entropies, and thermal free-energy corrections at 310 K. In separate runs, the initial structures were re-optimized with ωB97X-D [34] and the 6-31+G(d,p) basis set. The optimized geometries and energies of seven low-energy complexes are given as Supplementary data in Tables S1a-S7b. These calculations included dispersion interactions in the complexes, and the obtained energies were used to evaluate the electronic terms of the free energies. The calculated relative free energies included electronic, vibrational, and rotational terms at 310 K. Solvation free energies were calculated using the polarizable continuum model [35] for the water and methanol dielectric.

4. Results and discussion

Our investigations were focused on three sets of non-covalent complexes. In the first set, we generated complexes of phosphopep-

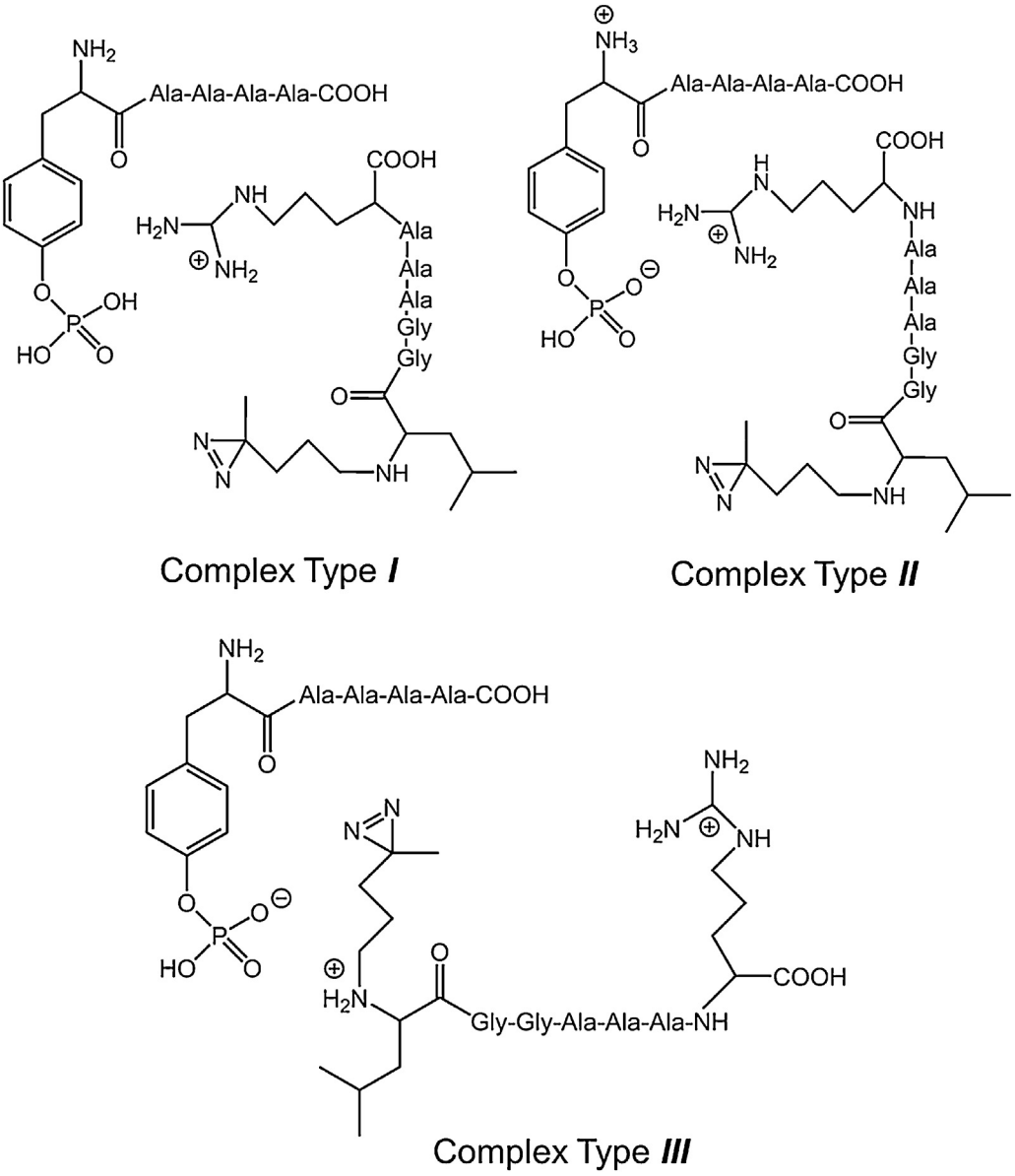

Fig. 2. Drawings of $(pYAAAA + {}^{*}LGGAAAR + H)^{+}$ protomer types I-III used in BOMD calculations.

tides pSAAAA, pTAAAA, and pYAAAA with the *N*-terminally tagged hepta- through nonapeptides $^{*}LGG(A)_nR$ ($n = 3–5$). For comparison, an analogous series of *N*-acetylated phosphopeptides, *N*-Ac-XAAAA (X = pSer, pThr, pTyr) was used. The purpose of *N*-acetylation was to block the formation of zwitterionic forms of the phosphopeptides and to investigate its effect on the complex formation and behavior. The third set consisted of combinations of pSAAAA, pTAAAA, and pYAAAA with the photoleucine (L*) containing hepta- through nonapeptides $L^{*}GG(A)_nR$ ($n = 3–5$). In addition to the different position of the diazirine ring in the *L and L* residues, the peptides also differ in their gas-phase basicity (GB), with the *L peptides having a secondary amine group, suggesting GB(*L) > GB(L*). For a general description, we use the previously introduced notation where the photopeptide and target peptide are denoted as M and m, respectively, and the complexes are labeled as $(m(M+H)^{+}$. Ions formed by photodissociative elimination of N_2 are denoted as $(mM–N_2 + H)^{+}$, $(M–N_2 + H)^{+}$ and $(m + H)^{+}$ for the respective surviving complex and peptide monomers formed upon dissociation.

The yields of gas-phase complexes formed by electrospray as singly charged ions were estimated as per cent mole fractions from the relative intensities of $(mM+H)^{+}$, $(M+H)^{+}$ and $(m + H)^{+}$ in the mass spectra [18,19]. The yields for combinations of pXAAAA and *N*-Ac-pXAAAA with $^{*}LGG(A)_nR$ ($n = 3–5$) ranged between 0.6–3.6%. In contrast, the yields of complexes from combinations of pXAAAA with $L^{*}GG(A)_nR$ ($n = 3–5$) were <0.1%. Doubly charged complexes were not observed for either series of peptides with intensities above the spectra threshold level. The yields of the more abundant complexes of the $^{*}LGG(A)_nR$ ($n = 3–5$) series were at the low end of those observed previously for complexes of hydrophobic peptides [16–19]. This finding was surprising, because the presumed phosphate-Arg interactions were expected to stabilize the complexes and increase their yields [10–12]. We note that an accurate evaluation of non-covalent complex yields for different sets of peptides can be difficult because of intrinsic differences in peptide concentrations. However, for the $^{*}LGG(A)_nR$ and $L^{*}GG(A)_nR$ series reported here we used the same phosphopeptide stock solutions to minimize effects of different concentrations. Thus, it appears that the $L^{*}GG(A)_nR$ peptides were unusually weak in forming complexes with the phosphopeptides. Complexes formed with yields >0.6% were further investigated by UVPD-MS^2 and CID-MS^3 exper-

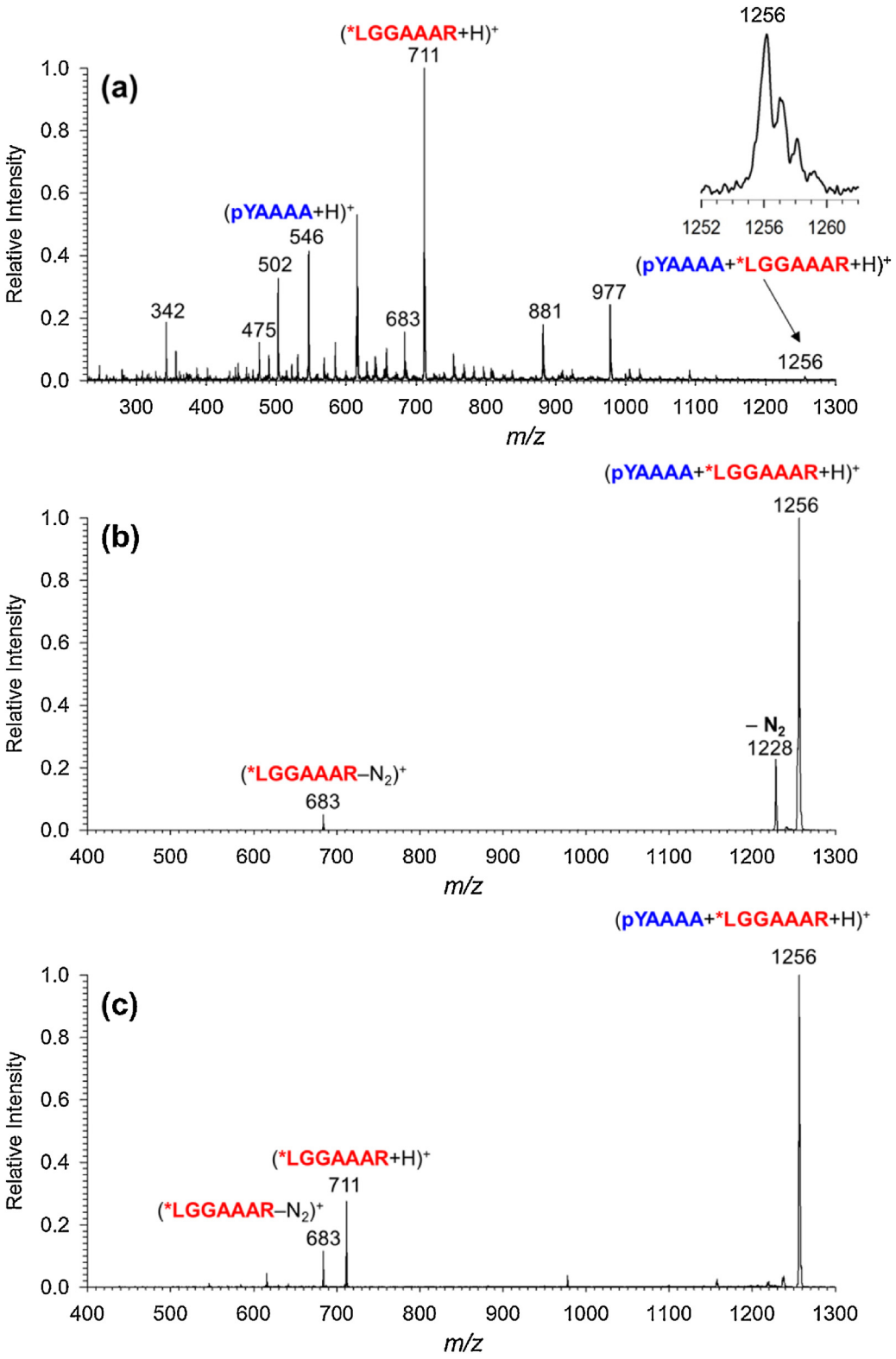

Fig. 3. (a) ESI-MS of a mixture of pYAAAA and *LGGAAAR showing the (pYAAAA + *LGGAAAR + H)$^+$ ion at *m/z* 1256 ; (b) UVPD-MS^2 spectrum of the *m/z* 1256 ion with 19 laser pulses; (c) CID-MS^2 spectrum of the *m/z* 1256 ion at normalized collision energy of 26 instrument units.

iments. For the L*GG(A)$_n$R series, the complex ion intensities were too low to allow us to obtain good quality MS^2 and MS^3 spectra.

Photodissociation of (m(M+H))$^+$ resulted in the formation of (mM–N_2 + H)$^+$ and peptide monomers. The latter were exclusively represented by the (M–N_2 + H)$^+$ ions because of the higher basicity of the Arg-containing peptides that retained the charging proton. The experimental results are illustrated for the complex ion (pYAAAA + *LGGAAAR + H)$^+$ (*m/z* 1256). The spectrum in Fig. 3a showed the ESI formation of the ion complex. The ion complexes can be stored in the ion trap for over 1 s without dissociation. UVPD resulted in loss of N_2, forming the (mM–N_2 + H)$^+$ photoproduct

Table 1
$R(MS^2)$ fractions of $(mM–N_2 + H)^+$ ions surviving photodissociation.

Peptide	$R(MS^2)$[a]		
	*LGG$(A)_3$R	*LGG$(A)_4$R	*LGG$(A)_5$R
pSAAAA	75	81	88
pTAAAA	80	81	86
pYAAAA	91	92	95
N-Ac-pSAAAA	90	89	89
N-Ac-pTAAAA	88	89	88
N-Ac-pYAAAA	79	80	84

[a]Percent fractions, see text for definition.

(*m/z* 1228, Fig. 3b) which underwent partial dissociation to the $(*L\text{-}N_2)GGAAAR + H)^+$ monomer (*m/z* 683, Fig. 3b). Remarkably, there

was less than 1% elimination of H_3PO_4 from the $(mM–N_2 + H)^+$ ions as illustrated in Fig. 3b. Similar results were obtained for all other pY, pS, and pT containing complexes. In contrast to photodissociation, collision-induced dissociation (CID) of $(m(M+H))^+$ resulted in complex dissociation to $((M+H))^+$ (*m/z* 711, Fig. 3c) that was accompanied by $(M–N_2 + H)^+$ at *m/z* 683 while no $(mM–N_2 + H)^+$ was detected. The yields of $(mM–N_2+H)^+$ complexes surviving photodissociation were expressed as $R(MS^2)$ values: $R(MS^2) = 100 \times [mM–N_2 + H]^+/\{[mM–N_2 + H]^+ + [M–N_2 + H]^+\}$ where square brackets indicate ion intensities in the UVPD-MS^2 spectra (Table 1). The fractions of $(mM–N_2 + H)^+$, expressed as $R(MS^2)$, combined contributions from non-covalent complexes surviving the exothermic loss of nitrogen [22] and their cross-linked isomers. The Table 1 data indicated high levels of retention of non-covalent complexes that exceeded 75%. Some minor trends of $R(MS^2)$ were observed in dependence on the photopeptide molecular size where increasing the number of Ala residues resulted in a slight increase of the fraction of non-dissociating complexes. This trend and its magnitude are consistent with the degree-of-freedom effect on the complex dissociation kinetics. For example, the internal degrees of freedom in (pYAAAA + *LGG$(A)_n$R + H)$^+$ increased by 11% from 516 for $n = 3$ to 576 for $n = 5$, a relatively minor change. The internal energies in the $(mM–N_2 + H)^+$ ions immediately after photodissociation are composed of the precursor $(m(M+H))^+$ ion internal energy and the exothermicity of N_2 elimination. The distribution of thermal vibrational energies at the ion trap temperature of 310 K was calculated for the (pYAAAA + *LGGAAAR + H)$^+$ complexes (Figure S1, Supplementary data), giving mean energy values of 258–261 kJ mol^{-1} for two conformers. An N_2 elimination from the diazirine ring followed by carbene isomerization to an olefin is ca. 200 kJ mol^{-1} exothermic [22], increasing the mean vibrational energy of $(mM–N_2 + H)^+$ ions to ca. 460 kJ mol^{-1} in the non-covalent complexes to drive their dissociation. In spite of this substantial excitation, only a minor fraction of complexes dissociated upon UVPD (Table 1), raising the question of covalent versus non-covalent bonding in the photoproducts. The fractions of non-covalent and covalently cross-linked complexes were then analyzed by CID.

The surviving $(mM–N_2 + H)^+$ photoproduct ion complexes were selected by mass and further investigated by CID-MS^3. The results

Table 3
Summed relative intensities of covalently cross-linked fragment ions in the UVPD-CID-MS^3 spectra of $(mM–N_2 + H)^+$ ions from (pXAAAA + *LGG$(A)_n$R + H)$^+$ complexes.

Phosphopeptide	%Relative Intensity[a]		
	Cross-Linked Fragment Ions		
	$(A)_3$[b]	$(A)_4$[c]	$(A)_5$[d]
pSAAAA	48	80	89
pTAAAA	44	71	50
pYAAAA	11	87	92

[a]Sums of relative intensities of fragment ions with *m/z* between that of the $(M–N_2 + H)^+$ and $(mM–N_2 + H)^+$ that originated from cross-linked complexes. [b]$(A)_3$ stands for complexes with *LGG$(A)_3$R; [c]$(A)_4$ stands for complexes with *LGG$(A)_4$R; [d]$(A)_5$ stands or complexes with *LGG$(A)_5$R.

for the (pXAAAA + *LGG$(A)_n$R + H)$^+$ ion complexes and their *N*-acetylated analogues are summarized in Tables 2 and 3. The $(M–N_2)$ photopeptides are abbreviated as $(A)_3$, $(A)_4$, and $(A)_5$ according to the number of Ala residues. The relative intensities of $(M–N_2 + H)^+$ monomer ions were taken as representing the fractions of non-covalent complexes. This followed from the general feature of CID spectra (Fig. 3c) showing that non-covalent complexes exclusively dissociated to monomers. Starting with the *N*-acetylated

phosphopeptides, CID-MS^3 analysis indicated that major fractions of the complexes (>90%) dissociated to monomeric peptides, as indicated by the data in the $(M–N_2 + H)^+$ columns in Table 2. As discussed below, these dissociations can chiefly originate from non-covalent complexes but also can include cross-links at the pX phosphate oxygens. The fractions of these complexes did not show strong dependence on the length of the photopeptide chain. Regarding covalent cross-linked complexes, their minor fractions were represented by fragment ions formed either by loss of H_3PO_4 from $(mM–N_2 + H)^+$, or resulted as H_3PO_4 adducts onto the $(M–N_2+H)^+$ moiety, as shown for the (pXAAAA + $(A)_4$ + H)$^+$ complexes (Fig. 4a,b,c). Note that none of these reactions was observed in the absence of photodissociation and so they can be unambiguously assigned to covalently cross-linked products.

Higher fractions of both the covalent cross-links and a variety of dissociation reactions were observed for photodissociation of complexes with pXAAAA having free *N*-termini. This was inferred from the CID-MS^3 spectra considering fragment ions with *m/z* between that of the $(M–N_2 + H)^+$ and $(mM–N_2 + H)^+$ that can be unambiguously assigned to originate from covalent cross-links. Rather than listing the multitude of individual cross-linked fragment ions for each combination of the phospho- and photopeptide, we summed their relative intensities that are presented in Table 3.

The CID-MS^3 data differed for pSAAAA, pTAAAA, and pYAAAA in both the nature of CID fragmentations and dependence on the length of the photopeptide. The fragmentations are illustrated by CID-MS^3 spectra of (pXAAAA + $(A)_4$ + H)$^+$ complexes (Fig. 5a–c). CID-MS^3 of the pSAAAA complexes resulted in loss of H_3PO_4 (*m/z* 1125 in Fig. 5a) and formation of $(M–N_2 + H_3PO_4 + H)^+$ fragment ions that appeared at *m/z* 852 in Fig. 5a and were incrementally shifted by 71 Da for the complexes with *LGGAAAR, denoted by $(A)_3$, and

Table 2
Relative fragment ion intensities in the UVPD-CID-MS^3 spectra of $(mM–N_2 + H)^+$ ions from (*N*-Ac-pXAAAA + *LGG$(A)_n$R + H)$^+$ complexes.

Peptide	Relative Intensity (%)								
	$(M–N_2+H)^+$			$(M–N_2+H_3PO_4+H)^+$			$(mM–N_2–H_3PO_4+H)^+$		
	$(A)_3$[a]	$(A)_4$[b]	$(A)_5$[c]	$(A)_3$	$(A)_4$	$(A)_5$	$(A)_3$	$(A)_4$	$(A)_5$
N-Ac-pSAAAA	94	92	91	3.7	3.5	4.8	2.4	4.2	3.9
N-Ac-pTAAAA	96	94	96	2.2	1.8	1.9	1.8	3.5	1.8
N-Ac-pYAAAA	98	97	90						

[a]$(A)_3$ stands for complexes with *LGG$(A)_3$R. [b]$(A)_4$ stands for complexes with *LGG$(A)_4$R. [c]$(A)_5$ stands or complexes with *LGG$(A)_5$R.

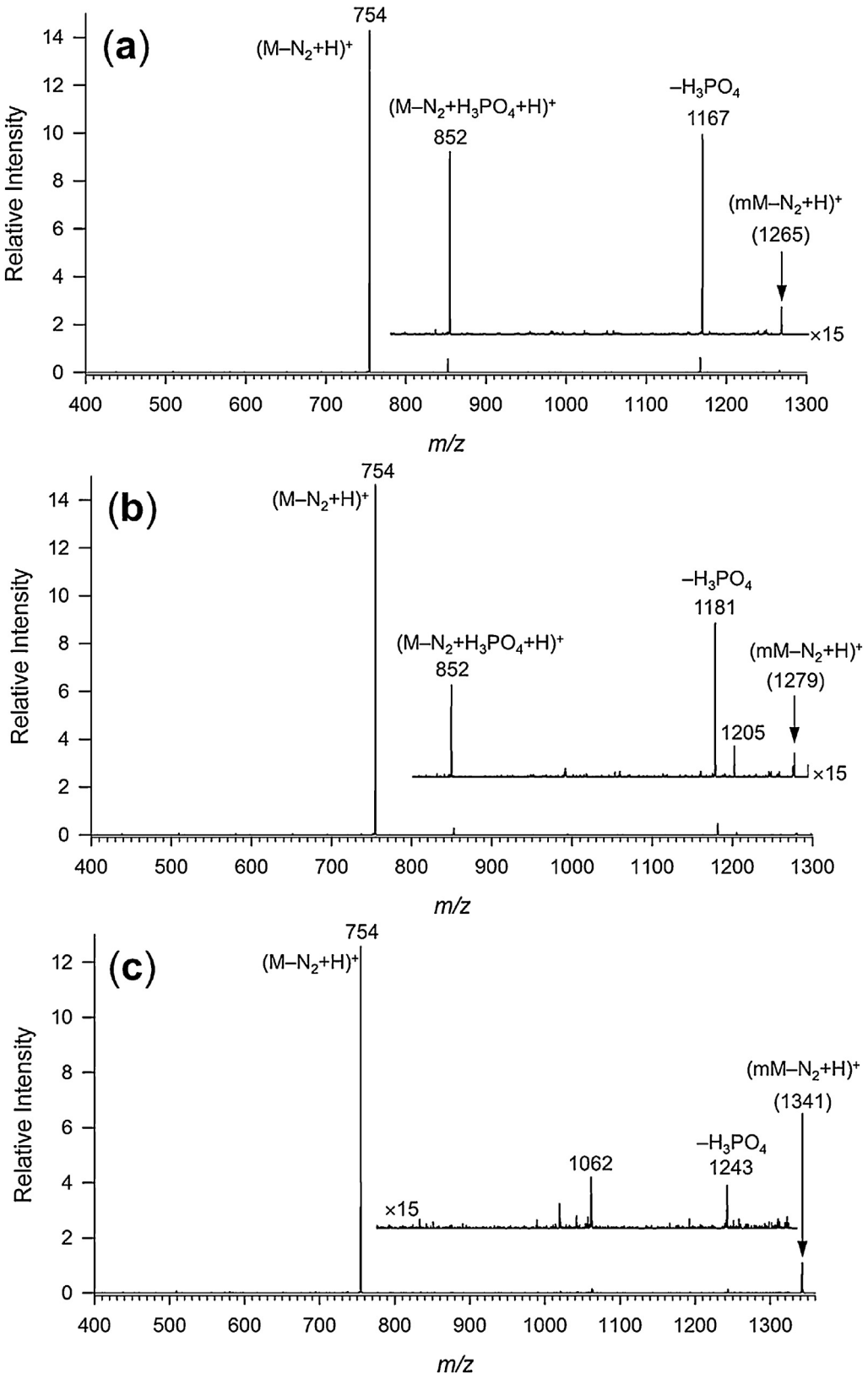

Fig. 4. CID-MS^3 spectra of (mM–N_2+H)$^+$ ions from UVPD of *LGGAAAAR complexes with (a) *N*-Ac-pSAAAA (*m/z* 1265), (b) *N*-Ac-pTAAAA (*m/z* 1279), and (c) *N*-Ac-pYAAAA (*m/z* 1341).

*LGGAAAR, denoted by $(A)_5$. These ions represented complexes in which the pSer phosphate group migrated onto the photopeptide as a result of cross-linking. In addition, CID-MS^3 of pSAAAA complexes with $(A)_3$, $(A)_4$, $(A)_5$ showed elimination of 134 Da (*m/z* 1089 in Fig. 5a) that we tentatively assign to a combined elimination of H_3PO_4 and two water molecules. Loss of 162 Da (*m/z* 1061 in Fig. 5a), possibly consecutive CO elimination after loss of 134 Da, was also abundant in the CID-MS^3 spectra of the pSAAAA complexes.

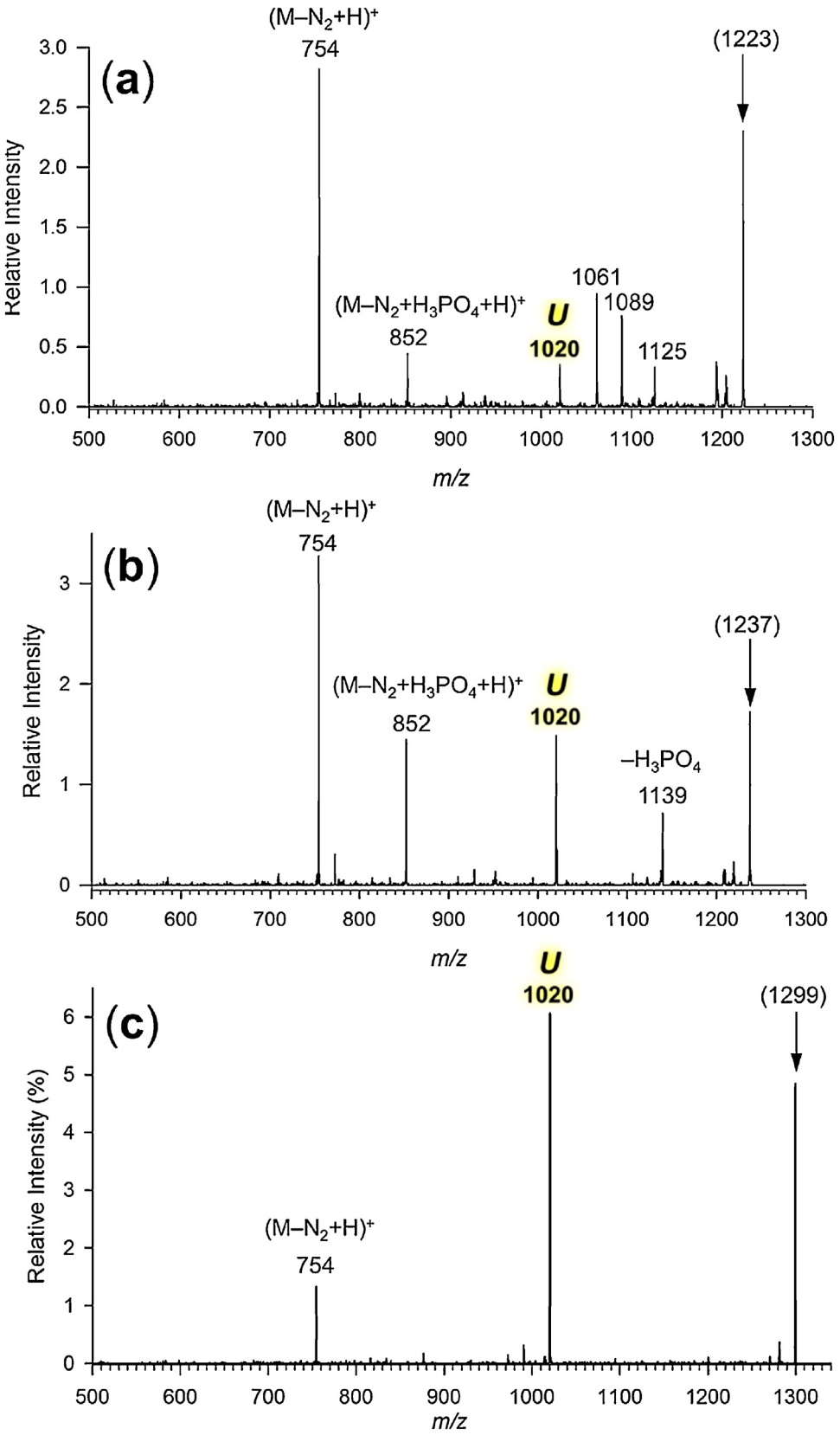

Fig. 5. CID-MS^3 spectra of (pXAAAA + $(A)_4$ + H)$^+$ complexes with: (a) pSAAAA (*m/z* 1223); (b) pTAAAA (*m/z* 1237); (c) pYAAAA (*m/z* 1299). The highlighted fragment ions at *m/z* 1020 are denoted as ***U*** and discussed in main text.

The relative abundance of these two dissociations gradually increased from the $(A)_3$ to $(A)_4$ and further on to $(A)_5$ complexes where they become prominent, representing 39 and 34% of the total fragment ion intensity. CID-MS^3 of the pTAAAA complexes showed mainly loss of H_3PO_4 (*m/z* 1139 in Fig. 5b) and formation of $(M–N_2 + H_3PO_4 + H)^+$ fragment ions (*m/z*

852 for the complex with $(A)_4$). Interestingly, dissociations analogous or homologous to the loss of 134 and 162 Da neutral fragments in the pSer series were absent for the pThr complexes.

A conspicuous feature of the CID-MS^3 spectra was the formation of cross-linked fragment ions at *m/z* 949, 1020, and 1091 from the respective $(A)_3$, $(A)_4$, and $(A)_5$ complexes (Figures S2-S4, Supplementary data). These fragment ions, which are highlighted and labeled ***U*** in the CID-MS^3 spectra (Fig. 5a,b,c), showed the same *m/z* when formed from the pSAAAA, pTAAAA, and pYAAAA complexes, indicating that the Ser, Thr and Tyr residues were eliminated by dissociation, so that covalent cross-linking must have taken place within the AAAA sequence of the phosphopeptides. At the same time, the pertinent neutral losses of 203, 217, and 279 Da from the phosphopeptides were difficult to explain by including the intact pSer (168 Da), pThr (182 Da) and pTyr (244 Da) moieties, because there was no logical mass unit to account for the missing 35 Da difference. Hence, we concluded that prior to or in the course of dissociation, the $(mM–N_2 + H)^+$ ion complexes underwent HPO_3 migration onto the photopeptide. The recipient group could not be determined by CID-MS^4 of the ***U*** ions (*m/z* 1020 from the complexes with *LGG$(A)_4$R) because of the substantially diminished ion count after the MS^3 step. We tentatively suggest that HPO_3 moved to one of the potentially nucleophilic groups in the photopeptides, which are the Arg guanidine and the (*L–N_2) secondary amine. The overall dissociation leading to the formation of ***U*** fragment ions can be tentatively explained as proceeding with backbone cleavage next to the Ala-2 residue in the rearranged phosphopeptide. The formation of ***U*** fragment ions relatively increased from $(A)_3$ to $(A)_4$ complexes and then leveled off.

In summarizing this section, we note that the CID-MS^3 dissociations of the photolyzed complexes indicated substantial fractions of covalently cross-linked products with the phosphopeptides with free *N*-termini. A common feature of the complexes was phosphate transfer from the phosphopeptide to the photopeptide. Although detailed mechanisms of the cross-linked ion dissociations remain to be elucidated, the above described reactive interactions between the phosphopeptide and photopeptide moieties provide a firm evidence for covalent bond formation in the complexes upon diazirine photodissociation.

We note that CID-induced phosphate migration among serine residues in phosphopeptide cations and anions has been reported and discussed by Reid and coworkers [36], and its importance for phosphoproteome analysis has been debated [37–40]. Collision-induced transfer of HPO_3 [41] and H_2SO_4 [42] in non-covalent complexes of phosphorylated and sulfated peptides has been reported. In contrast to the previous studies, we did not observe phosphate transfer upon CID of non-covalent (pXAAAA + *LGG$(A)_n$R + $H)^+$ complexes prior to photodissociative cross-linking.

5. Complex ion structures and dynamics

In order to shed light on the interactions in the complexes, we undertook a detailed computational study of the (pYAAAA + *LGGAAAR + $H)^+$ ion. BOMD of several Type I, II, and III protomeric complexes (Fig. 2), followed by gradient geometry optimization, furnished several structures representing local energy minima at 0 K. The structures were sorted out by free energies to select lowest energy representatives of each protomeric type, as summarized in Table 4. The gas-phase energies varied, depending on the DFT method used, and further adjustments were made by including gas-phase enthalpies, entropies, and solvation energies [35]. Regarding the latter, solvation in the water and methanol dielectrics gave practically identical results, and thus only the water data are reported. Because of all these effects, we used a rather broad energy range of 40 kJ mol^{-1} to include protomeric complexes that can be produced by electrospray and represented in the gas phase. Type I complexes in which the phosphopeptide was in a neutral canonical form (Fig. 2) were represented by a single low-energy structure (**1**, Fig. 6) The main non-covalent interactions between pYAAAA and *LGGAAAR in **1** originated from hydrogen bonding to the phosphoester and carboxyl groups of the phoshopeptide. Two other low-energy structures that were started as Type I underwent prototropic rearrangements upon gradient optimization, yielding Type III complexes **2** and **3** with a deprotonated phosphate and two protonation sites on the basic groups in *LGGAAAR (Fig. 6). The main non-covalent interactions between the peptide moieties in **2** and **3** involved hydrogen bonding of the charged groups to the phosphate anion, as well as neutral amide-amide hydrogen bonds. The single low-energy Type II complex was represented by structure **4** (Fig. 6). The phosphate anion in **4** was internally solvated by neutral amide and carboxyl groups, whereas the charged groups received internal solvation within the photopeptide. Type III complexes were most frequently represented among the low-energy structures, as illustrated by structures **5** and **6**, in addition to **2** and **3**. The phosphate anion in **5** received internal solvation from the $(A)_3$ neutral amide and carboxyl groups. The secondary ammonium group on *L participated in hydrogen bonding to the phosphopeptide carboxyl whereas the charged Arg group was solvated internally within the $(A)_3$ moiety. Structure **6** showed a yet different pattern of non-covalent interactions. Both charged groups in $(A)_3$ were involved in hydrogen bonding to the phosphate anion, and the non-covalent binding of the peptides was further strengthened by neutral hydrogen bonds between the amide groups (Fig. 6). Finally, structure **7** developed from an initial Type III complex that rearranged by proton migration from the $(A)_3$ carboxyl onto the phosphate group. The main non-covalent interactions between pXAAAA and $(A)_3$ in **7** involved hydrogen bonding of the neutral phosphoester group, as well as the ammonium group on *L (Fig. 6).

Table 4
Relative energies of (pYAAAA + *LGGAAR + $H)^+$ complexes in the gas phase and aqueous solution.

Complex[d]	Type[e]	Relative Energy[a]					
		B3LYP[b]			ωB97X-D[c]		
		$\Delta H_{g,0}$	$\Delta G_{g,310}$[f]	ΔG_{aq}[g]	$\Delta H_{g,0}$	$\Delta G_{g,310}$[f]	ΔG_{aq}[g]
1	I	32	19	19	59	46	35
2	I[h]	42	36	36	35	28	25
3	I[h]	60	46	46	38	23	6
4	II	54	56	56	34	36	25
5	III	94	79	79	97	83	27
6	III	0	0	0	0	0	0
7	III	41	38	38	40	37	36

[a]In kJ mol^{-1} including B3LYP/6–31 G(d,p) zero-point energies and referring to 0 K unless stated otherwise. [b]Gas-phase structures fully optimized with the 6–31 G(d,p) basis set. [c]Gas-phase structures fully optimized with the 6-31+G(d,p) basis set. [d]See Fig. 6 and Tables S1a-S7b for ωB97X-D/6-31+G(d,p) optimized structures. [e]See Fig. 2 for the Type definition. [f]Relative free energies in the gas-phase at 310 K. [g]Including solvation free energies in a polarizable dielectric continuum of water. [h]Rearranged to Type III complexes upon gradient optimization.

With these low-energy structures in hand, we investigated their long (100 ps) BOMD trajectories with the goal of determining close contacts of the incipient carbene with X—H bonds in the target pYAAAA peptide, resulting from intra-complex thermal motion at the ion trap temperature (310 K). A close contact of the carbene with an X—H bond is prerequisite for the chemical reaction forming the new covalent X—C bond and resulting in cross-linking. A lack of contact favors carbene isomerization to an unreactive olefin. Hence, the percentage of time the diazirine spends in close contacts with X—H bonds is indicative of the propensity for cross-linking. Close contacts obtained for the C–H, N—H, and O—H bonds in pYAAAA were grouped by amino acid residues. With pY, close contacts with the

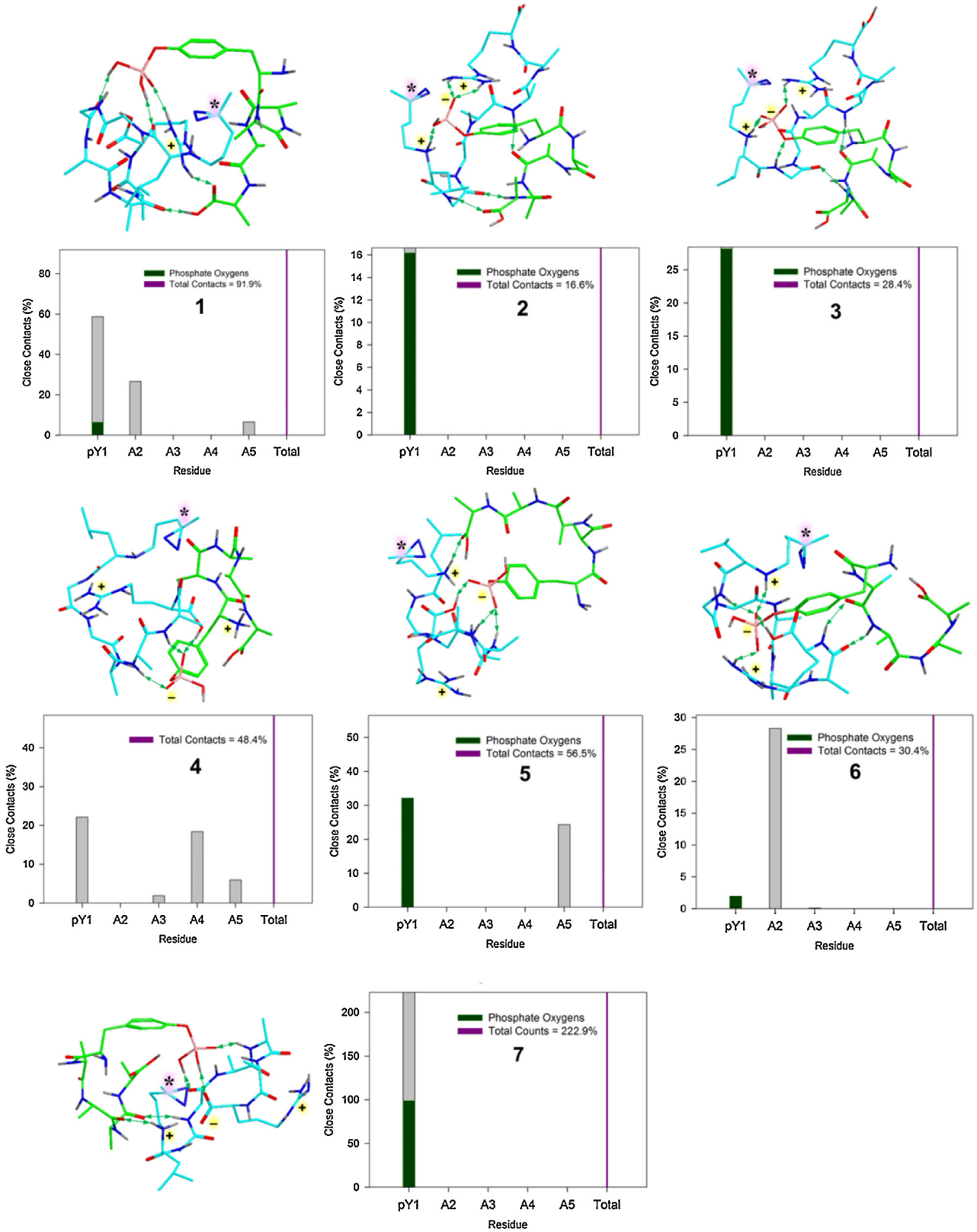

Fig. 6. ωB97X-D/6-31+G(d,p) optimized structures of low-energy complexes **1**-**7**. Atom color coding is as follows: Green or cyan = C, gray = H, blue = N, red = O, bronze = P. Only exchangeable (N—H, O—H) hydrogens are shown. Graphs of close contact distributions in complexes **1**-**7**. Magenta bars: Total percentage of all contacts at pYAAAA. Simultaneous contacts with multiple atoms in the target peptide account for the count exceeding 100%. Gray bars: contacts at X-H of the given amino acid residue. Green bars: contacts with pY phosphate O-H. (For interpretation of the references to colour in this figure legend, the reader is referred to the web version of this article).

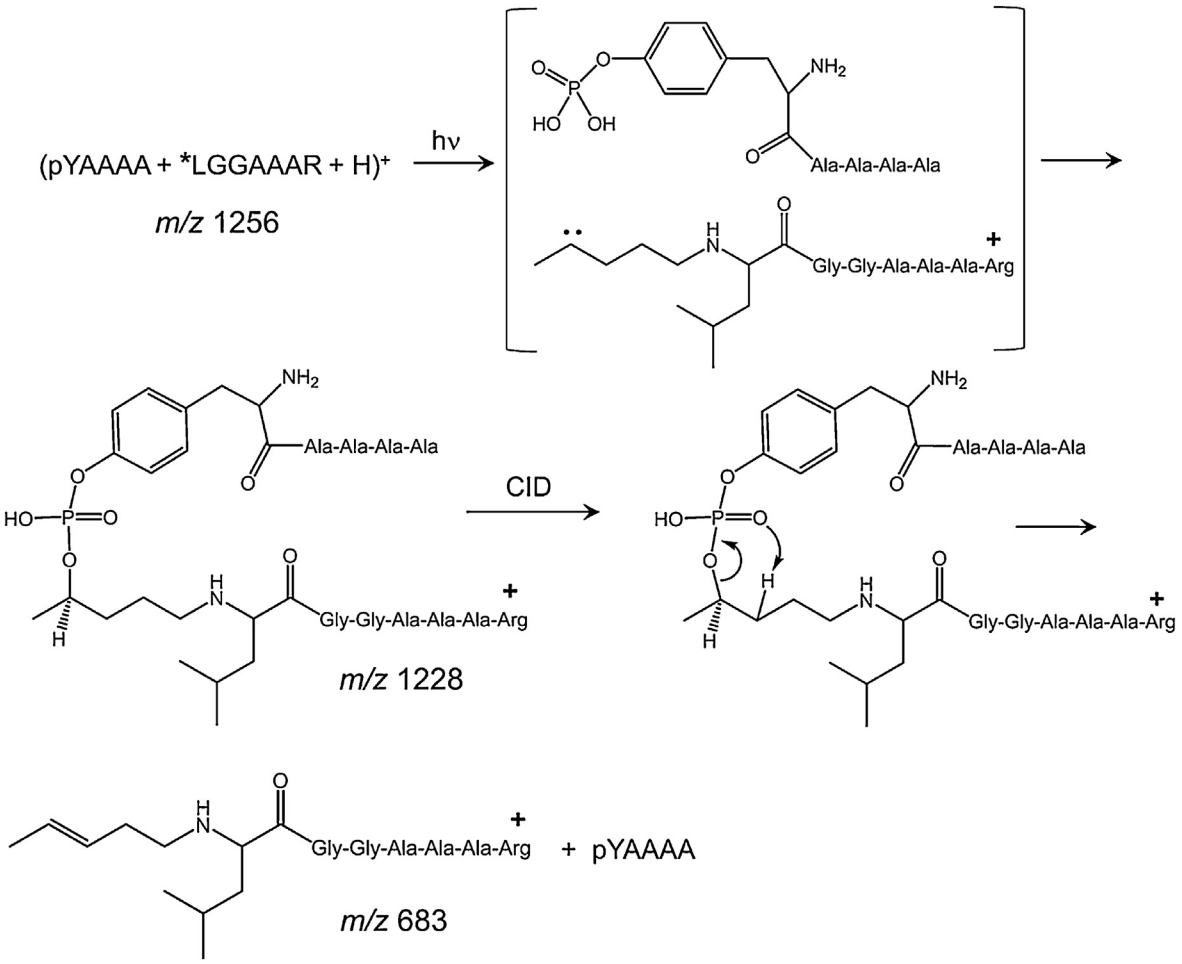

Scheme 1. Proposed mechanism for the formation of phosphate cross-linked complexes.

phosphate oxygens were counted as a specific subgroup. The close-contact data analysis allowed us to distinguish different groups of complexes. Thermal motion in structures **2** and **3** resulted in exclusive close contacts with the phosphate oxygens in 16.6 and 28.4% of the 100 ps trajectory time. The relatively low contact counts resulted from the rigid arrangement of the *L ammonium cation solvating the phosphate anion in **2** and **3** that was not disrupted by thermal motion at 310 K. Consequently, the conformational space for the diazirine tag was limited, allowing it to reach the phosphate group only. Complexes **1** and **4** displayed contacts in 91.9 and 48.4% of trajectory time, respectively. Both trajectories indicated contacts with pY but mostly off the phosphate group. Additionally, a fraction of contacts with pYAAAA in **1** and **4** involved the Ala2 and Ala5 residues. Complexes **5** and **7** had substantial contacts in the pY residue. In particular, complex **7** allowed for simultaneous multiple contacts with pY X—H bonds upon thermal motion, reaching it 222.9% of trajectory time. A significant fraction of these contacts were with the phosphate oxygens. Complex **6** showed a lower count of close contacts at 30.4% of trajectory time. The contacts chiefly involved the Ala2 residue of pYAAAA. The reason for the low count and selective contacts in this case can be seen in the rigid arrangement of the solvating groups around the phosphate anion. This fixed the position of the *L ammonium cation while allowing access of the diazirine tag to a limited conformational space, chiefly including the Ala2 residue.

The results of the close contact analysis for the low-energy conformers of (pYAAAA + *LGGAAAR + H)$^+$ are now discussed in relation to the CID-MS^3 spectra and the derived cross-linking data. Upon UVPD, the complex exhibited 91% of non-dissociating ions (Table 1), consisting of cross-links and surviving non-covalent complexes. CID-MS^3 of (mM–N_2 + H)$^+$ resulted in 89% dissociation to (M–N_2 + H)$^+$, 8% formation of the ***U*** fragment ion, and 3% of combined loss of NH_3 and HPO_3, composing the 11% yield of cross-linked ions (Table 3). Out of the low-energy complexes, structures **2**, **3**, **5**, and **7** displayed frequent close contacts with the pY phosphate oxygens. Carbene insertion into the P—O—H bond can produce phosphodiester intermediates linking the pY residue to the *N*-terminal side chain (Scheme 1). However, such cross-links were expected to undergo standard phosphate elimination upon CID, reversing the results of the photochemical cross-linking reaction and leading to peptide separation. Hence, the 89% fraction of (M–N_2 + H)$^+$ may include cross-links to the phosphate group. We note that a similar conclusion has been reached by Iacobucci, Sinz, and coworkers for carbene-peptide crosslinks to COOH groups forming CID-labile ester bonds [43]. This interpretation is consistent with the observation that the fraction of (M–N_2 + H)$^+$ increased upon increasing the normalized collision energy in CID of the (mM–N_2 + H)$^+$ ions. Analysis of structures **3** and 5 indicated frequent close contacts with the Ala4 and Ala5 residues in pYAAAA. These can account for cross-linking away from the pY residue and be consistent with the formation upon CID of the ***U*** fragment ions by elimination of the Tyr residue after phosphate transfer onto the $(A)_3$ moiety. Mechanistic details of these processes are yet to be elucidated.

The (pYAAAA + *LGGA$_n$R + H)$^+$ complexes displayed a conspicuous trend for the formation of the ***U*** ions that greatly increased with

the length of the photopeptide (Figure S2, Supplementary data), as also illustrated by the 11% to 92% increase of the total fraction of cross-linked fragment ions (Table 3). The ***U*** ions involve cross-linking at the A3-A5 residues in pYAAAA. Although we did not carry out detailed calculations of these larger systems, the above-described analysis of the (pYAAAA + *LGGAAAR + H)$^+$ structures can be used for interpretation. The formation of ***U*** fragment ions competes with cross-linking to the pY phosphate group that is facilitated by hydrogen bonding to the Arg and *N*-terminal charged groups in the complexes. As the photopeptide sequence length is increased, simultaneous coordination to the pY phosphate of the Arg and *N*-terminal charged groups becomes entropically disfavored, because there is a large number of alternative hydrogen bonding sites for pY, forming conformers of comparable free energy. This should increase close contacts of the diazirine group with the C-terminal residues in pYAAAA and favor cross-linking in positions remote from the pY phosphate.

Another conspicuous result revealed by the present study was the large negative effect on cross-linking of *N*-terminal acetylation in all pXAAAA peptides (Table 2). This may result from a combination of a steric effect of the *N*-acetyl group, hindering hydrogen bonding at the phosphopeptide *N*-terminus, and its diminished basicity that would disfavor zwitterionic protomers of the phosphopeptide.

Finally, we note that the current complexes of pXAAAA with *LGG(A)$_n$R displayed rather contrasting features regarding their formation by electrospray and ion stability in the gas phase. When compared to complexes of more hydrophobic peptides, studied previously [18,19], pXAAAA and *LGG(A)$_n$R showed much less efficient formation of gas-phase complexes by electrospray. The low yields were even more dramatic for the pXAAAA complexes with L*GG(A)$_n$R. On the contrary, when formed in the gas phase, the (pXAAAA + *LGG(A)$_n$R + H)$^+$ complexes displayed substantial resistance (75–95%, Table 2) to dissociation to peptide components following diazirine photolysis. This by far exceeded the typical stabilities of complexes composed of hydrophobic peptides that range between 19–44% [18]. These comparisons clearly point to the negative effect of solvent on the stability of the (pXAAAA + *LGG(A)$_n$R + H)$^+$ complexes. Both the complexes and their polar peptide components can be stabilized by solvation in aqueous solution to balance the relative enthalpies at equilibrium, whereby complex dissociation is favored by entropy. In the absence of solvent, the break up of the attractive charge-dipole interactions between the polar phosphate, arginine, and N-terminal groups in the complexes is much less compensated by polar interactions within the components, and the dissociation is hindered even after excitation by photolysis and carbene rearrangement.

6. Conclusions

Photodissociative loss of N_2 from non-covalent complexes of pXAAAA phoshopeptides with peptides tagged at the *N*-terminus and containing a single arginine residue produced large (75–95%) fractions of stable surviving adducts. The distribution of non-covalent and covalently cross-linked photoproducts was found to depend on several factors, such as the photopeptide chain length, nature of phosphorylated amino acid residue, and phosphopeptide *N*-terminal modification. CID of the photoproducts revealed H_3PO_4 transfer onto the photopeptide followed by unusual backbone dissociations in the phosphopeptide residue. Structure analysis by density functional theory and Born-Oppenheimer molecular dynamics trajectory calculations indicated dominant polar interactions in the complexes involving the charged arginine, *N*-terminal, and phosphate groups.

Acknowledgments

Financial support from the Chemistry Division of the National Science Foundation (Grants CHE-1661815 for experiments and CHE-1624430 for calculations) is gratefully acknowledged. F.T. thanks the Klaus and Mary Ann Saegebarth Endowment for general support.

Appendix A. Supplementary data

Supplementary material related to this article can be found, in the online version, at doi:https://doi.org/10.1016/j.ijms.2018.09.037.

References

[1] E.H. Fischer, E.G. Krebs, J. Biol. Chem. 216 (1955) 121–132.
[2] P. Cohen, Nat. Cell Biol. 4 (2002) E127–E130.
[3] M.A. McKercher, X. Guan, Z. Tan, D.S. Wuttke, Proteins 86 (2018) 164–176.
[4] K.A. Schug, W. Lindner, Chem. Rev. 105 (2005) 67–113.
[5] G. Waksman, D. Kominos, S.C. Robertson, N. Pant, D. Baltimore, R.B. Birge, D. Cowburn, H. Hanafusa, B.J. Mayer, M. Overduin, et al., Nature 358 (1992) 646–653.
[6] S.M. Pascal, T. Yamazaki, A.U. Singer, L.E. Kay, J.D. Forman-Kay, Biochemistry 34 (1995) 11353–11362.
[7] J.A. Loo, Mass Spectrom. Rev. 16 (1997) 1–23.
[8] J.A. Loo, P. Hu, P. McConnell, W.T. Mueller, T.K. Sawyer, V. Thanabal, J. Am. Soc. Mass Spectrom. 8 (1997) 234–243.
[9] K.A. Sannes-Lowery, P. Hu, D.P. Mack, H.-Y. Mei, J.A. Loo, Anal. Chem. 69 (1997) 5130–5135.
[10] A.S. Woods, S. Ferre, J. Proteome Res. 4 (2005) 1397–1402.
[11] S.N. Jackson, S.C. Moyer, A.S. Woods, J. Am. Soc. Mass Spectrom. 19 (2008) 1535–1541.
[12] A.S. Woods, S.C. Moyer, S.N. Jackson J. Proteome Res. 7 (2008) 3423–3427.
[13] J. Laskin, Z. Yang, A.S. Woods, Phys. Chem. Chem. Phys. 13 (2011) 6936–6946.
[14] M. Suchanek, A. Radzikowska, C. Thiele, Nat. Methods 2 (2005) 261–268.
[15] T. Yang, X.-M. Li, X. Bao, Y.M.E. Fung, D. Li, Nat. Chem. Biol. 12 (2016) 70.
[16] R. Pepin, C.J. Shaffer, F. Turecek, J. Mass Spectrom. 52 (2017) 557–560.
[17] Y. Liu, Z. Ramey, F. Tureček, Chem. Eur. J. 24 (2018) 9259–9263.
[18] H.T.H. Nguyen, P.C. Andrikopoulos, L. Rulíšek, C.J. Shaffer, F. Tureček, J. Am. Soc. Mass Spectrom. 30 (2018) 1706–1720.
[19] C.J. Shaffer, P.C. Andrikopoulos, J. Řezáč, L. Rulíšek, F. Tureček, J. Am. Soc. Mass Spectrom. 27 (2016) 633–645.
[20] M.T.H. Liu, Chemistry of Diazirines, Vols. I and II, CRC Press, Boca Raton, FL, 1987.
[21] C.J. Shaffer, J. Martens, A. Marek, J. Oomens, F. Tureček, J. Am. Soc. Mass Spectrom. 27 (2016) 1176–1185.
[22] A. Marek, F. Tureček, J. Am. Soc. Mass Spectrom. 25 (2014) 778–789.
[23] J.M. Janz, Y. Ren, R. Looby, M.A. Kazmi, P. Sachdev, A. Grunbeck, L. Haggis, D. Chinnapen, A.Y. Lin, C. Seibert, T. McMurry, K.E. Carlson, T.W. Muir, S. Hunt, T.P. Sakmar, J. Am. Chem. Soc. 133 (2011) 15878–15881.
[24] C.J. Shaffer, A. Marek, R. Pepin, K. Slováková, F. Tureček, J. Mass Spectrom. 50 (2015) 470–475.
[25] H.T.H. Nguyen, C.J. Shaffer, F. Tureček, J. Phys. Chem. B 119 (2015) 3948–3961.
[26] C.J. Shaffer, A. Marek, H.T.H. Nguyen, F. Tureček, J. Am. Soc. Mass Spectrom. 26 (2015) 1367–1381.
[27] H.J. Berendsen, J.V. Postma, W.F. van Gunsteren, A.R.H.J. DiNola, J.R. Haak, J. Chem. Phys. 81 (1984) 3684–3690.
[28] J. Rezac, J. Fanfrlík, D. Salahub, P. Hobza, J. Chem. Theory Comput. 5 (2009) 1749–1760.
[29] J.J.P. Stewart, MOPAC 16; Stewart Computational Chemistry: Colorado Springs, CO, USA.
[30] J. Řezáč, Cuby – Ruby Framework for Computational Chemistry, Version 4 http://cuby4.molecular.cz.
[31] J. Řezáč, J. Comput. Chem. 37 (2016) 1230–1237.
[32] M.J. Frisch, G.W. Trucks, H.B. Schlegel, G.E. Scuseria, M.A. Robb, J.R. Cheeseman, G. Scalmani, V. Barone, G.A. Petersson, H. Nakatsuji, M. Caricato, A.V. Marenich, J. Bloino, B.G. Janesko, R. Gomperts, B. Mennucci, H.P. Hratchian, J.V. Ortiz, A.F. Izmaylov, J.L. Sonnenberg, D. Williams-Young, F. Ding, F. Lipparini, F. Egidi, J. Goings, B. Peng, A. Petrone, T. Henderson, D. Ranasinghe, V.G. Zakrzewski, J. Gao, N. Rega, G. Zheng, W. Liang, M. Hada, M. Ehara, K. Toyota, R. Fukuda, J. Hasegawa, M. Ishida, T. Nakajima, Y. Honda, O. Kitao, N. Nakai, T. Vreven, K. Throssell, J.A. Montgomery Jr, J.E. Peralta, F. Ogliaro, M.J. Bearpark, J.J. Heyd, E.N. Brothers, K.N. Kudin, V.N. Staroverov, T.A. Keith, R. Kobayashi, J. Normand, K. Raghavachari, A.P. Rendell, J.C. Burant, S.S. Iyengar, J. Tomasi, M. Cossi, J.M. Millam, M. Klene, C. Adamo, R. Cammi, J.W. Ochterski, R.L. Martin, K. Morokuma, O. Farkas, J.B. Foresman, J.D. Fox, Gaussian 16, Revision A01, Gaussian, Inc., Wallingford CT, 2016.
[33] A.D. Becke, Phys. Rev. A 38 (1988) 3098–3100.
[34] J.D. Chai, M. Head-Gordon, Phys. Chem. Chem.Phys. 10 (2008) 6615–6620.

[35] J. Tomasi, B. Mennucci, R. Cammi, Quantum mechanical continuum solvation models, Chem. Rev. 105 (2005) 2999–3093.
[36] L. Cui, I. Yapici, B. Borhan, G.E. Reid, J. Am. Soc. Mass Spectrom. 25 (2014) 141–148.
[37] L. Cui, G.E. Reid, Proteomics 13 (2013) 964–973.
[38] N.M. Riley, J.J. Coon, Anal. Chem. 88 (2016) 74–94.
[39] N.B. Borotto, N. Degraan-Weber, Y. Zhou, R.W. Vachet, J. Am. Soc. Mass Spectrom. 25 (2014) 1739–1746.
[40] A.M. Palumbo, S.A. Smith, C.L. Kalcic, M. Dantus, P.M. Stemmer, G.E. Reid, Mass Spectrom. Rev. 30 (2011) 600–625.
[41] A.M. Palumbo, G.E. Reid, Anal. Chem. 80 (2008) 9735–9747.
[42] A.L. Patrick, N.C. Polfer, Anal. Chem. 87 (2015) 9551–9554.
[43] C. Iacobucci, M. Gotze, C. Piotrowski, C. Arlt, A. Rehkamp, C. Ihling, C. Hage, A. Sinz, Anal. Chem. 90 (2018) 2805–2809.